Title	Valence hole subbands and optical gain spectra of GaN/Ga1-xAlxN strained quantum wells
Author(s)	Fan, Weijun; Li, M. F.; Chong, T. C.
Citation	Fan, W., Li, M. F., Chong, T. C., & Xia, J. B. (1996). Valence hole subbands and optical gain spectra of GaN/Ga1-xAlxN strained quantum wells. Journal of applied physics, 80(6), 3471.
Date	1996
URL	http://hdl.handle.net/10220/18007
Rights	© 1996 American Institute of Physics. This paper was published in Journal of Applied Physics and is made available as an electronic reprint (preprint) with permission of American Institute of Physics. The paper can be found at the following official DOI: [http://dx.doi.org/10.1063/1.363217]. One print or electronic copy may be made for personal use only. Systematic or multiple reproduction, distribution to multiple locations via electronic or other means, duplication of any material in this paper for a fee or for commercial purposes, or modification of the content of the paper is prohibited and is subject to penalties under law.

Valence hole subbands and optical gain spectra of GaN/$Ga_{1-x}Al_xN$ strained quantum wells

W. J. Fan, M. F. Li,[a] and T. C. Chong
Center for Optoelectronics, Department of Electrical Engineering, National University of Singapore, Singapore 119260

J. B. Xia
National Laboratory for Superlattices and Microstructures, Institute of Semiconductors, Academia Sinica, Beijing 100083, People's Republic of China

(Received 4 March 1996; accepted for publication 30 May 1996)

The valence hole subbands, TE and TM mode optical gains, transparency carrier density, and radiative current density of the zinc-blende GaN/$Ga_{0.85}Al_{0.15}N$ strained quantum well (100 Å well width) have been investigated using a 6×6 Hamiltonian model including the heavy hole, light hole, and spin-orbit split-off bands. At the $k=0$ point, it is found that the light hole strongly couples with the spin-orbit split-off hole, resulting in the so+lh hybrid states. The heavy hole does not couple with the light hole and the spin-orbit split-off hole. Optical transitions between the valence subbands and the conduction subbands obey the $\Delta n=0$ selection rule. At the $k\neq 0$ points, there is strong band mixing among the heavy hole, light hole, and spin-orbit split-off hole. The optical transitions do not obey the $\Delta n=0$ selection rule. The compressive strain in the GaN well region increases the energy separation between the **so1**+lh1 energy level and the hh1 energy level. Consequently, the compressive strain enhances the TE mode optical gain, and strongly depresses the TM mode optical gain. Even when the carrier density is as large as 10^{19} cm^{-3}, there is no positive TM mode optical gain. The TE mode optical gain spectrum has a peak at around 3.26 eV. The transparency carrier density is 6.5×10^{18} cm^{-3}, which is larger than that of GaAs quantum well. The compressive strain overall reduces the transparency carrier density. The J_{rad} is 0.53 kA/cm^2 for the zero optical gain. The results obtained in this work will be useful in designing quantum well GaN laser diodes and detectors. © *1996 American Institute of Physics.* [S0021-8979(96)08417-4]

I. INTRODUCTION

The wide energy gap III-V nitride semiconductors GaN, AlN, and their quantum well structures have received considerable attention for their device applications in the blue and ultraviolet wavelengths.[1–18] Recently, the successful fabrication of the blue light III-V nitride semiconductor laser was first demonstrated by Nakamura.[1] The vast majority of research on III-V nitrides has been focused on the wurtzite crystal phase. The reason is that most of III-V nitrides have been grown on sapphire substrates which generally transfer their hexagonal symmetry to the nitride film. Nevertheless, interest in zinc-blende nitrides has been growing recently.[2–6] The zinc-blende GaN has a higher saturated electron drift velocity and a somewhat lower energy gap than wurtzite GaN.[7]

In this work, the effective mass approximation is used to calculate valence hole subbands and the TE and TM mode optical gains of the zinc-blende GaN/$Ga_{0.85}Al_{0.15}N$ strained quantum well. In bulk zinc-blende GaN and AlN, the spin-orbit split-off at the top of the valence band is around 17 meV.[19] Therefore, the 4×4 valence band effective mass Hamiltonian of Broido and Sham[20] is not suitable for the calculation and the spin-orbit split-off band must also be taken into consideration. People *et al.*[21] developed a 6×6 valence-band Hamiltonian in the calculation of strained bulk semiconductor layers. Meney *et al.*[22] compared the valence band structure calculated by 4×4, 6×6, and 8×8 models, respectively. The influence from the conduction band to the valence band can be neglected because III-V nitride semiconductors have larger energy gaps. We modify the 6×6 Hamiltonian of People *et al.* to investigate the valence hole subband structures, optical gain, and radiative current density of the zinc-blende GaN/$Ga_{0.85}Al_{0.15}N$ strained quantum well. In Sec. II, the 6×6 Hamiltonian is used to calculate the hole subband energies, wavefunctions, and density of states. The hole subbands are found to be far from parabolic and very anisotropic. Therefore, the axial approximation and the simple parabolic band approximation are not suitable for this case. We use numerical calculation methods and the Cray J916 supercomputer with very long computation time to obtain reliable and accurate results, rather than using any analytical approximation. In Sec. III, the method and the numerical calculation results of optical transition matrix elements between the conduction subbands and the valence subbands are described. In Sec. IV, the numerical calculation method of carrier density is given. In Sec. V, the TE and TM mode optical gains are calculated respectively. Discussion of the results and comparison with other work are given.

II. CALCULATION METHOD AND VALENCE HOLE SUBBANDS

The 6×6 Hamiltonian in Ref. 21 is modified to investigate the valence hole subband structures of zinc-blende

[a]Electronic mail: elelimf@nus.sg

$GaN/Ga_{0.85}Al_{0.15}N$ strained multiquantum wells (MQW) grown on (001)-oriented substrates. Following Luttinger,[23] we shall deal with the negative of valence electron Hamiltonian in our analysis. The Hamiltonian of the MQW is therefore given by

$$H_{SL}^{v}=\begin{array}{c} \begin{matrix} j=1, & 2, & 3, & 4, & 5, & 6, \\ (3/2,3/2), & (3/2,1/2), & (3/2,-1/2), & (3/2,-3/2), & (1/2,1/2), & (1/2,-1/2), \end{matrix} \\ \begin{bmatrix} H+V(z) & \alpha & \beta & 0 & i\alpha/\sqrt{2} & -i\sqrt{2}\beta \\ \alpha^* & L+V(z) & 0 & \beta & -i[D/\sqrt{2}-\sqrt{2}E] & i\sqrt{3/2}\alpha \\ \beta^* & 0 & L+V(z) & -\alpha & -i\sqrt{3/2}\alpha^* & -i[D/\sqrt{2}-\sqrt{2}E] \\ 0 & \beta^* & -\alpha^* & H+V(z) & -i\sqrt{2}\beta^* & -i\alpha^*/\sqrt{2} \\ -i\alpha^*/\sqrt{2} & i[D/\sqrt{2}-\sqrt{2}E] & i\sqrt{3/2}\alpha & i\sqrt{2}\beta & S+V(z) & 0 \\ i\sqrt{2}\beta^* & -i\sqrt{3/2}\alpha^* & i[D/\sqrt{2}-\sqrt{2}E] & i\alpha/\sqrt{2} & 0 & S+V(z) \end{bmatrix} \end{array}, \tag{1}$$

where

$$H=\frac{\hbar^2}{2m_0}[(k_x^2+k_y^2)(\gamma_1+\gamma_2)+k_z^2(\gamma_1-2\gamma_2)]-E(z),$$

$$L=\frac{\hbar^2}{2m_0}[(k_x^2+k_y^2)(\gamma_1-\gamma_2)+k_z^2(\gamma_1+2\gamma_2)]+E(z),$$

$$\alpha=\frac{\hbar^2}{2m_0}2\sqrt{3}[k_z(ik_y-k_x)\gamma_3],$$

$$\beta=\frac{\hbar^2}{2m_0}\sqrt{3}[2ik_xk_y\gamma_3-(k_x^2k_y^2)\gamma_2],$$

$$D=\frac{\hbar^2}{2m_0}[2(k_x^2+k_y^2)\gamma_2-4k_z^2\gamma_2], \tag{2}$$

$$S=\frac{\hbar^2}{2m_0}[(k_x^2+k_y^2+k_z^2)\gamma_1]+\Delta_0,$$

$$E(z)=\begin{cases} -\frac{2}{3}D_u(1+2c_{12}/c_{11})e_{xx}, & in\ \ well, \\ 0, & in\ \ barrier, \end{cases}$$

$$V(z)=\begin{cases} V_0, & in\ \ barrier, \\ 0, & in\ \ well. \end{cases}$$

$V(z)$ is the periodic potential of MQW, $\frac{2}{3}D_u$ is the valence-band uniaxial deformation potential, Δ_0 is the spin-orbit split-off energy, m_0 is the free-electron mass, and γ_1, γ_2, γ_3 are the Luttinger parameters. We assume that the MQW is grown on a thick $Ga_{0.85}Al_{0.15}N$ buffer layer, so that a compressive strain exits only in the GaN well region. The in-plane strain $e_{xx}=(a-a_0)/a_0$, where a is the unstrained lattice constant of $Ga_{0.85}Al_{0.15}N$ and a_0 the unstrained lattice constant of GaN. c_{11} and c_{12} are elastic stiffness constants.

The six dimensional hole envelope wave function for the MQW can be expanded as

$$\phi_{n_v,k}=\{\phi^j_{n_v,k}\}, \quad (j=1,2,\ldots 6.), \tag{3}$$

where

$$\phi^j_{n_v,k}=\exp[i(k_xx+k_yy)]\sum_m a^j_{n_v,k,m}\frac{1}{\sqrt{L}}\exp\left[i\left(k_z+m\frac{2\pi}{L}\right)z\right], \tag{4}$$

and $L=l+d$ is the period of the MQW, where l and d are the widths of the wells and the barriers, respectively.

In order to distinguish the heavy hole (hh), light hole (lh), and spin-orbit band (so) components in the MQW wave function, we introduce the following probability functions:

$$P^{\rm hh}(n_v,k)=\sum_{j=1,4}\sum_m a^{j*}_{n_v,k,m}a^j_{n_v,k,m}$$

$$P^{\rm lh}(n_v,k)=\sum_{j=2,3}\sum_m a^{j*}_{n_v,k,m}a^j_{n_v,k,m} \tag{5}$$

$$P^{\rm so}(n_v,k)=\sum_{j=5,6}\sum_m a^{j*}_{n_v,k,m}a^j_{n_v,k,m}.$$

From $P^{\rm hh}(n_v,k),P^{\rm lh}(n_v,k),P^{\rm so}(n_v,k)$, we can estimate the respective components of the heavy hole, light hole and spin-orbit split-off states in the MQW state $\phi_{n_v,k}$. Note that the following sum rule holds,

$$\sum_i P^i_{(n_v,k)}=1, \quad i=\text{hh,lh,so}. \tag{6}$$

We use Eqs. (1) and (2) to calculate the valence band structures of $GaN/Ga_{0.85}Al_{0.15}N$ strained quantum well. The lattice constants of GaN and AlN are 4.50 and 4.35 Å, respectively.[4] The lattice constant of $Ga_{0.85}Al_{0.15}N$ is 4.4775 Å obtained by linear interpolation. The corresponding compressive strain is 0.5% in the well region. The well width is 100 Å, the barrier width is 200 Å. We use the spin-orbit split-off Δ_0 value of 17 meV[19] for the well and barrier. The experimental measured energy gap at the Γ point of zinc-blende GaN is 3.2 eV.[2] We take the calculated energy gap at the Γ point of zinc-blende AlN to be 5.94 eV,[24,25] and the band offset $\Delta E_c/\Delta E_v=70/30$,[26] so the $\Delta E_c=288$ meV and $\Delta E_v=123$ meV for $GaN/Ga_{0.85}Al_{0.15}N$ quantum well using linear interpolation. Other parameters used in this work are listed in Table I. The conduction subbands of the quantum

TABLE I. Parameters used in the calculation.

Luttinger parameters γ_1, γ_2, γ_3 (Ref. 24)	3.07, 0.80, 1.26
Elastic stiffness c_{11}, c_{12} (Gpa) (Ref. 8)	296, 154
Deformation potential D_d^{cv}, $\frac{2}{3}D_u^v$ (eV) (Ref. 24)	−7.7, 1.6
Electron effective mass m_e for GaN (m_0) (Ref. 27)	0.15
Refractive index n (Ref. 9)	2.2
Intraband relaxation time τ (ps) (Ref. 28)	0.1
Lattice constants for GaN, AlN(Å) (Ref. 4)	4.50, 4.35
Spin-orbit split-off Δ_0 (meV) (Ref. 19)	17
Energy gaps E_g (Γ) for GaN (Ref. 2), AlN (eV) (Ref. 24)	3.2, 5.94
Band offset $\Delta E_c/\Delta E_v$ (Ref. 26)	70/30

well are calculated by the simple parabolic band approximation using electron effective mass in Table I.

Figure 1 shows the in-plane dispersion curves of the valence hole subbands of the $GaN/Ga_{0.85}Al_{0.15}N$ compressive strained quantum well calculated by the 6×6 model. Figure 2 shows the corresponding wave functions of the energy levels at $k=0$ in Fig. 1. Figure 3 shows the variation of hh, lh, and so components in each subband state versus the in-plane wave vector. From Fig. 3, we can see that the hh does not couple with lh and so at $k=0$. Therefore, the states of $n=1$, 3, 5 at $k=0$ can be identified as hh1, hh2, and hh3 states, respectively. On the other hand, the lh state strongly couples with so state even at $k=0$.[29] According to Figs. 2 and 3, the states of $n=2$, 4, 6 at $k=0$ can be identified as **so1**+lh1, **so2**+lh2, and **so3**+lh3 states, respectively. At the $k\neq 0$ points, there is band mixing among the heavy hole, light hole, and spin-orbit split-off states due to the contribution of the nondiagonal parts in Eq. (1). Figure 4 shows the in-plane dispersion curves of the valence hole subbands of $GaN/Ga_{0.85}Al_{0.15}N$ quantum well where strain effect is neglected [$D_u=0$ in Eq. (2)]. Comparing Fig. 1 with Fig. 4, the hybrid state **lh1**+so1 (with **lh1** dominant) changes into the **so1**+lh1 state (with **so1** dominant) when the strain effect is taken into consideration.

We have compared that in the case of 200 Å barrier width, there is almost no interaction between the neighboring well and no energy dispersion along the z direction. Therefore, the result obtained can also be used for the case of single quantum well structure.

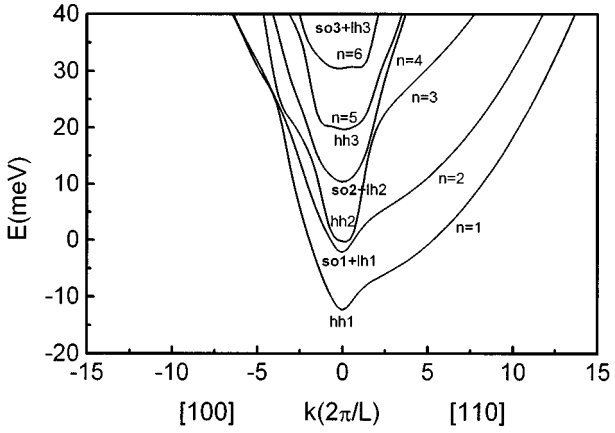

FIG. 1. The in-plane dispersion curves of the valence hole subbands of $GaN/Ga_{0.85}Al_{0.15}N$ compressively strained quantum well.

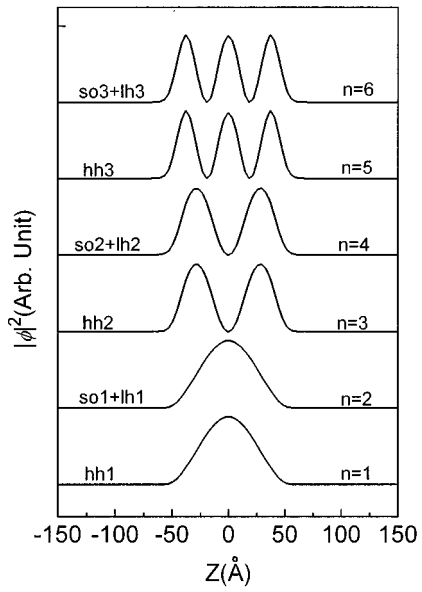

FIG. 2. The wave functions of the hole subband energy levels at $k=0$ of $GaN/Ga_{0.85}Al_{0.15}N$ strained quantum well.

III. OPTICAL TRANSITION MATRIX ELEMENTS

The optical transition matrix elements for transitions between the valence hole subbands and the conduction electron subbands are given by:[30,31]

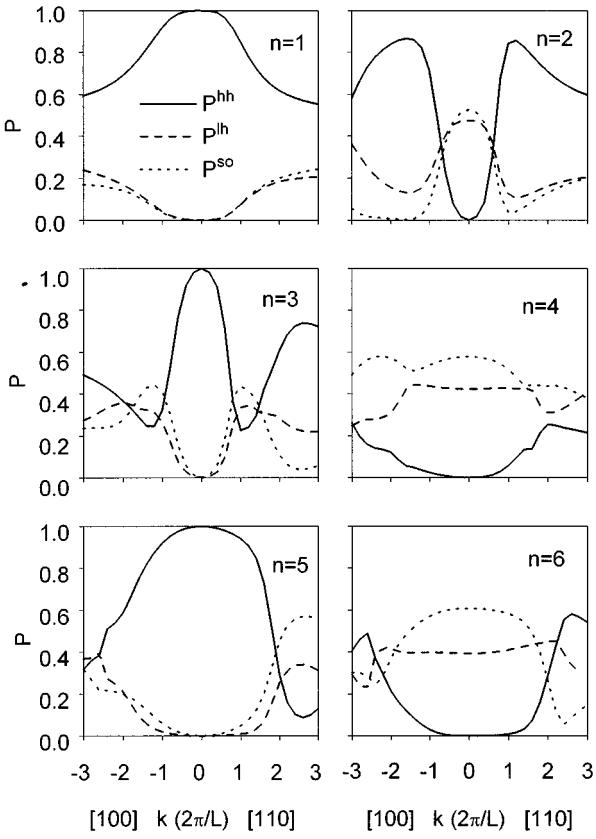

FIG. 3. The variation of the hh, lh, and so components in each state of $GaN/Ga_{0.85}Al_{0.15}N$ strained quantum well vs the in-plane wave vector.

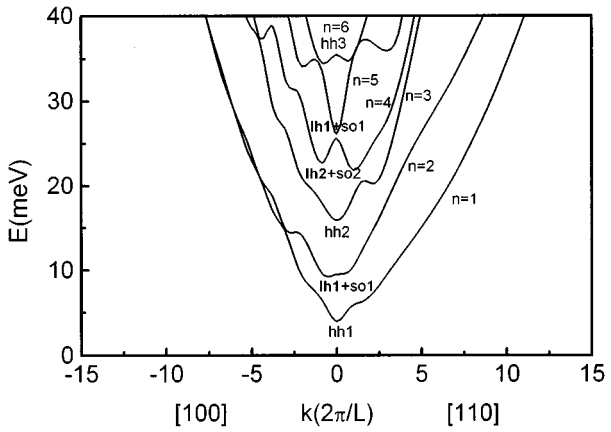

FIG. 4. The in-plane dispersion curves of the valence hole subbands of $GaN/Ga_{0.85}Al_{0.15}N$ quantum well without strain.

$$M_i^{n_v n_c} = \langle \Psi_{n_v,k} | \hat{p}_i | \Phi_{n_c,k} \rangle, \quad i = x,y,z, \tag{7}$$

where, $\hat{p}_i$ is the momentum operator, $\Phi_{n_c,k}$ and $\Psi_{n_v,k}$ are the actual electron and hole wave functions, respectively. The spin-orbit-coupling wave functions of the valence band at the Γ point are[21]

$$\begin{aligned}
\left|\frac{3}{2},\frac{3}{2}\right\rangle &= \frac{1}{\sqrt{2}}|(X+iY)\uparrow\rangle, \\
\left|\frac{3}{2},\frac{1}{2}\right\rangle &= \frac{i}{\sqrt{6}}|[(X+iY)\downarrow -2Z\uparrow]\rangle, \\
\left|\frac{3}{2},-\frac{1}{2}\right\rangle &= \frac{1}{\sqrt{6}}|[(X-iY)\uparrow +2Z\downarrow]\rangle, \\
\left|\frac{3}{2},-\frac{3}{2}\right\rangle &= \frac{i}{\sqrt{2}}|(X-iY)\downarrow\rangle, \\
\left|\frac{1}{2},\frac{1}{2}\right\rangle &= \frac{1}{\sqrt{3}}|[(X+iY)\downarrow +Z\uparrow]\rangle, \\
\left|\frac{1}{2},-\frac{1}{2}\right\rangle &= \frac{i}{\sqrt{3}}|[-(X-iY)\uparrow +Z\downarrow]\rangle,
\end{aligned} \tag{8}$$

where, $|X\rangle$, $|Y\rangle$, $|Z\rangle$, and $|s\rangle$ are the orbital wave functions of the top of the valence band and the bottom of the conduction band, respectively. $\uparrow$ and $\downarrow$ denote spin-up or spin-down components. Therefore, the actual hole wave function $\Psi_{n_v,k}$ is the product of the hole envelope wave function in Eq. (3) and the spin-orbit-coupling wave functions of the top of the valence band in Eq. (8). The actual wave function of the conduction electron subands $\Phi_{n_c,k}$ can be expanded as:

$$\begin{aligned}
\Phi_{n_c,k} = \exp[i(k_x x + k_y y)] \sum_m d_{n_c,k,m} \frac{1}{\sqrt{L}} \\
\times \exp\left[i\left(k_z + m\frac{2\pi}{L} \right) z \right] |s\rangle.
\end{aligned} \tag{9}$$

Substituting Eqs. (3), (8), (9), into (7), we have

$$\begin{aligned}
M_x^{n_v n_c} &= \langle \Psi_{n_v,k} | \hat{p}_x | \Phi_{n_c,k}\uparrow \rangle + \langle \Psi_{n_v,k} | \hat{p}_x | \Phi_{n_c,k}\downarrow \rangle \\
&= p_0 \sum_m \left(\frac{1}{\sqrt{2}} a^1_{n_v,k,m} + \frac{i}{\sqrt{6}} a^2_{n_v,k,m} \right. \\
&\quad + \frac{1}{\sqrt{6}} a^3_{n_v,k,m} + \frac{i}{\sqrt{2}} a^4_{n_v,k,m} \\
&\quad \left. + \frac{1}{\sqrt{3}} a^5_{n_v,k,m} - \frac{i}{\sqrt{3}} a^6_{n_v,k,m} \right) d^*_{n_c,k,m},
\end{aligned} \tag{10}$$

$$\begin{aligned}
M_y^{n_v n_c} &= \langle \Psi_{n_v,k} | \hat{p}_y | \Phi_{n_c,k}\uparrow \rangle + \langle \Psi_{n_v,k} | \hat{p}_y | \Phi_{n_c,k}\downarrow \rangle \\
&= p_0 \sum_m \left(\frac{i}{\sqrt{2}} a^1_{n_v,k,m} - \frac{1}{\sqrt{6}} a^2_{n_v,k,m} \right. \\
&\quad - \frac{i}{\sqrt{6}} a^3_{n_v,k,m} + \frac{1}{\sqrt{2}} a^4_{n_v,k,m} \\
&\quad \left. + \frac{i}{\sqrt{3}} a^5_{n_v,k,m} - \frac{1}{\sqrt{3}} a^6_{n_v,k,m} \right) d^*_{n_c,k,m},
\end{aligned} \tag{11}$$

$$\begin{aligned}
M_z^{n_v n_c} &= \langle \Psi_{n_v,k} | \hat{p}_z | \Phi_{n_c,k}\uparrow \rangle + \langle \Psi_{n_v,k} | \hat{p}_z | \Phi_{n_c,k}\downarrow \rangle \\
&= p_0 \sum_m \left(-\frac{2i}{\sqrt{6}} a^2_{n_v,k,m} + \frac{2}{\sqrt{6}} a^3_{n_v,k,m} \right. \\
&\quad \left. + \frac{1}{\sqrt{3}} a^5_{n_v,k,m} + \frac{i}{\sqrt{3}} a^6_{n_v,k,m} \right) d^*_{n_c,k,m},
\end{aligned} \tag{12}$$

where, $p_0 = \langle s|p_x|X\rangle = \langle s|p_y|Y\rangle = \langle s|p_z|Z\rangle \cdot$ p_0 is given by[32,33]

$$|p_0|^2 = \left(\frac{m_0}{m_e} - 1 \right) \frac{(E_g + \Delta_0)}{2(E_g + \frac{2}{3}\Delta_0)} m_0 E_g. \tag{13}$$

E_g is the unstrained energy gap of GaN. m_e is the electron effective mass of GaN.

For a quantum well laser with well layer growth direction along z, M_z corresponds to the TM mode optical transition and M_x (or M_y) corresponds to the TE mode optical transition.[34] Figures 5 and 6 show the squared optical transition matrix elements for TE and TM modes transitions from the four valence subband energy levels ($n=1$–4) to the first conduction subband energy level as a function of k along the [100] direction for the $GaN/Ga_{0.85}Al_{0.15}N$ compressively strained quantum well. These results are obtained by numerical calculation of Eqs. (10)–(12). As indicated in Figs. 5 and 6, at the $k=0$ point, the optical transitions from the valence subband states to the conduction subband states obey the selection rule $\Delta n = 0$. The squared optical transition matrix elements for the TE mode are the sum of the major contribution from the electron to heavy hole transition and the minor contribution from the electron to hybrid state of light hole and spin-orbit split-off hole transition (Fig. 5). For the TM mode, the contribution comes from the electron to hybrid state of light hole and spin-orbit split-off hole transition only (Fig. 6). This is because M_x in Eq. (10) includes heavy

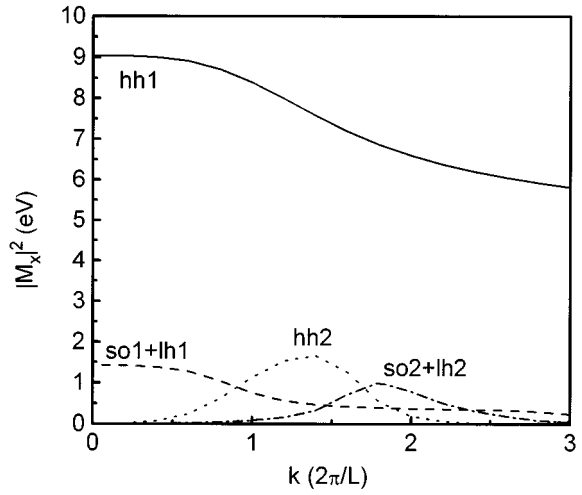

FIG. 5. The squared optical transition matrix elements for TE mode from the first conduction subband to the valence subbands as a function of k along the [100] direction for the $GaN/Ga_{0.85}Al_{0.15}N$ compressively strained quantum well.

hole, light hole, and spin-orbit split-off hole wave functions. However, M_z in Eq. (12) does not include heavy hole wavefunction. At the $k \neq 0$ points, the $\Delta n=0$ selection rule does not hold. There is band mixing between heavy hole, light hole, and spin-orbit split-off hole. Therefore, the squared optical transition matrix elements are the sum of the contribution from both electron to heavy hole and electron to hybrid state of light hole and spin-orbit split-off states.

IV. CARRIER DENSITY

The carrier density in a given band can be found for a given quasi-Fermi level by integrating the density of states

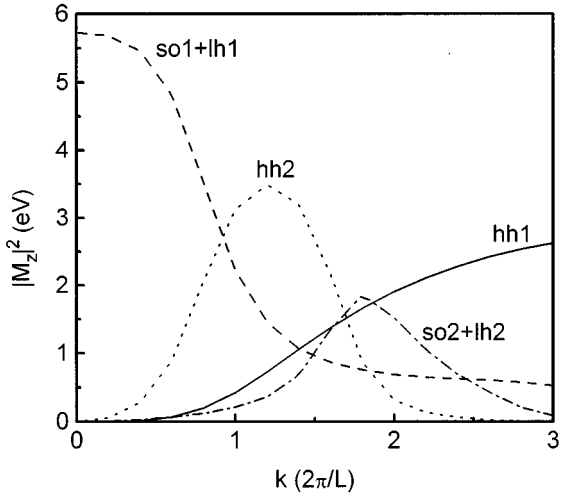

FIG. 6. The squared optical transition matrix elements for TM mode from the first conduction subband to the valence subbands as a function of k along the [100] direction for the $GaN/Ga_{0.85}Al_{0.15}N$ compressively strained quantum well.

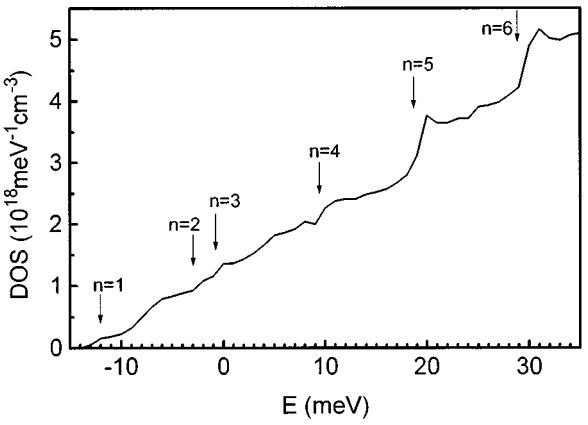

FIG. 7. The density of state for the valence hole subbands of the $GaN/Ga_{0.85}Al_{0.15}N$ compressively strained quantum well.

multiplied by the occupation probability over the entire band. For the parabolic subband in the conduction band, the electron concentration can be written as[32]

$$N=\frac{m_e k_B T}{\pi\hbar^2 l}\sum_{n_c} \ln\{1+\exp[-(E_{en_c}E_{fc})/k_B T]\}, \tag{14}$$

where k_B is the Boltzmann's constant, T is the temperature, m_e is the electron effective mass, E_{fc} is the electron quasi-Fermi level. The sum is over all quantized subbands within the conduction band of the quantum well, and the E_{en_c} are the quantized energy levels. For the valence band, the subband structure is far from parabolic, as indicated in Fig. 1. Equation (14) is no longer valid. Thus, for this case, it is more appropriate to find the carrier density by numerically integrating over k space. We have

$$P=\sum_{n_v} \int \frac{1}{4\pi^2 l} f_v[E_{hn_v}(k_x,k_y)]dk_x dk_y, \tag{15}$$

where E_{hn_v} is the hole energy (not the electron energy) in the valence subband. The Fermi–Dirac distributions for electrons in the conduction bands f_c and for holes (not for electron) in the valence subbands f_v are defined as

$$f_c=\frac{1}{1+\exp[(E_{en_c}-E_{fc})/k_B T]}, \tag{16}$$

$$f_v=\frac{1}{1+\exp[(E_{hn_v}-E_{fv})/k_B T]}, \tag{17}$$

where E_{fv} are the hole quasi-Fermi level in the valence band.

Figure 7 is the density of states (DOS) of the valence subbands for a quantum well obtained by numerical calculation. In Fig. 7, the density of states of the valence subbands is quite different from a step function predicted by simple parabolic subbands in a quantum well. This result is expected since the valence subbands are far from parabolic case and are highly anisotropy, as shown in Fig. 1. To check the reliability of our numerical calculation program, we have used our program to calculate the GaAs/AlGaAs 50 Å quantum well density of states, and compared with the result of Szmulowicz *et al.*[35] The density of state curves obtained by

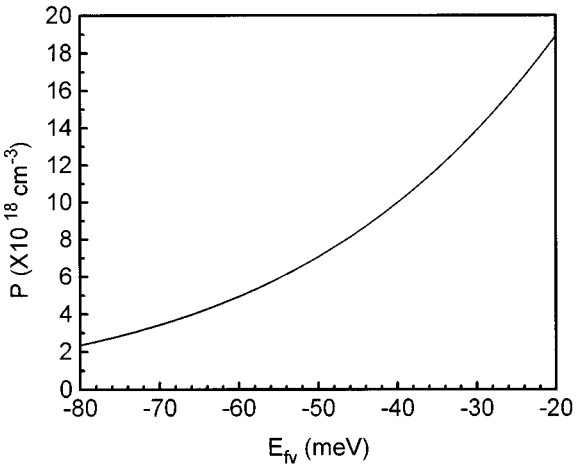

FIG. 8. The calculated hole concentration as a function of Fermi energy level for the GaN/$Ga_{0.85}Al_{0.15}N$ compressively strained quantum well at $T=300$ K.

us and obtained by Szmulowicz *et al.* are almost identical. Figure 8 shows the calculated hole concentration as a function of Fermi energy level E_{fv} for the GaN/$Ga_{0.85}Al_{0.15}N$ compressively strained quantum well at $T=300$ K.

V. OPTICAL GAIN AND RADIATIVE CURRENT DENSITY

According to the formula given in Refs. 32 and 36 and the definition of f_c, f_v in Eqs. (16) and (17), the optical gain can be written as

$$g(E)=\frac{\pi e^2\hbar}{m_0^2\varepsilon_0 ncE}\sum_{n_c,n_v}\int\int\frac{|M^{cv}|^2}{4\pi^2 l}[f_c+f_v-1]\times\frac{1}{\pi}\frac{\hbar/\tau}{(E_{eh}-E)^2+(\hbar/\tau)^2}dk_x dk_y, \tag{18}$$

where E is the photon energy, ϵ_0 is the free-space dielectric constant, n is a refractive index, c is the light velocity, τ is the intraband relaxation time. The transition energy E_{eh} is given by

$$E_{eh}=E_{en_c}+E_{hn_v}+E_g^s, \tag{19}$$

where

$$E_g^s=E_g+2D_d^{cv}(1-c_{12}/c_{11})e_{xx}, \tag{20}$$

D_d^{cv} is the interband hydrostatic deformation potential. $g(E)$ in Eq. (18) is also a function of carrier density. Using a specific electron density N, and charge neutrality condition $N=P$, from $N(E_{fc})$ and $P(E_{fv})$ curves obtained in Sec. IV, we obtain the values of D_{fc} and E_{fv}. Substituting Eqs. (16) and (17) into Eq. (18) and do the numerical calculation of Eq. (18), we obtain the value of $g(E)$.

The spontaneous emission rate can be given by[37]

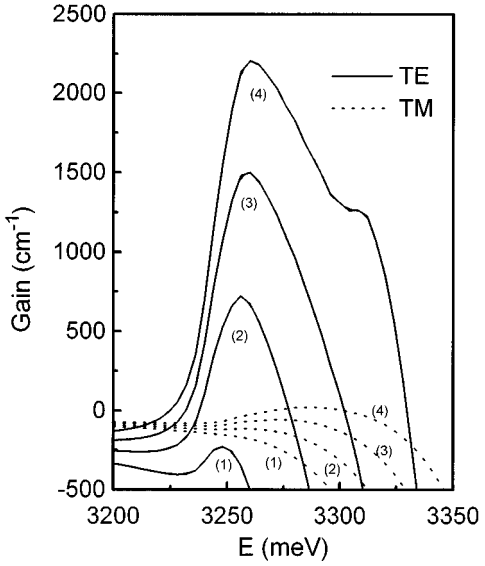

FIG. 9. Optical gain spectra at $T=300$ K for the GaN/$Ga_{0.85}Al_{0.15}N$ compressively strained quantum well at carrier densities, (1) $N=6\times10^{18}$ cm^{-3}, (2) 8×10^{18} cm^{-3}, (3) 10×10^{18} cm^{-3}, (4) 12×10^{18} cm^{-3}.

$$R_{sp}(E)=\frac{ne^2E}{\pi m_0^2\varepsilon_0\hbar^2c^3}\sum_{n_c,n_v}\int\int\frac{|M^{cv}|^2}{4\pi^2 l}f_c f_v\frac{1}{\pi}\times\frac{\hbar/\tau}{(E_{eh}-E)^2+(\hbar/\tau)^2}dk_x dk_y. \tag{21}$$

The radiative current density $J_{\rm rad}$ can be calculated from the spontaneous emission spectrum using[32]

$$J_{\rm rad}=el\int R_{sp}(E)dE. \tag{22}$$

A. Polarization dependence of laser light output

Figures 9 and 10 show the optical gain spectra at $T=300$ K for GaN/$Ga_{0.85}Al_{0.15}N$ quantum well with strain and without strain, respectively. Comparing Fig. 9 with Fig. 10, we

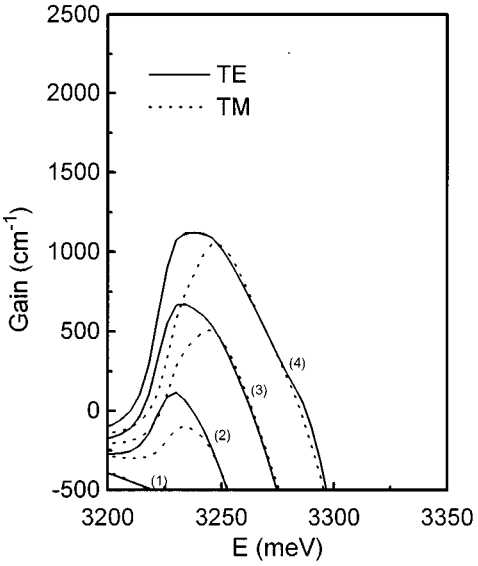

FIG. 10. Optical gain spectra at $T=300$ K for the GaN/$Ga_{0.85}Al_{0.15}N$ quantum well without strain at carrier densities, (1) $N=6\times10^{18}$ cm^{-3}, (2) 8×10^{18} cm^{-3}, (3) 10×10^{18} cm^{-3}, (4) 12×10^{18} cm^{-3}.

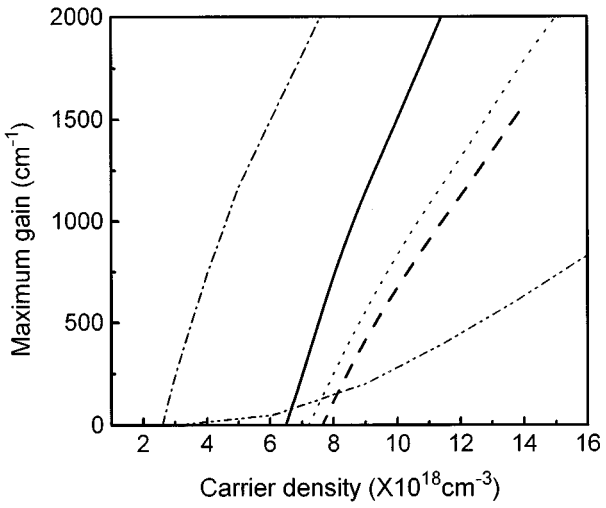

FIG. 11. Maximum optical gain of TE mode as a function of carrier density for the GaN/$Ga_{0.85}Al_{0.15}N$ compressively strained quantum well at $T=300$ K (solid line) and for the quantum well without strain (dashed line). We also show for comparison the maximum gain for an unstrained 100 Å GaN quantum well between $Al_{0.26}Ga_{0.74}N$ barriers (dot line) from Ref. 38, for a 100 Å GaAs/$Al_{0.4}Ga_{0.6}As$ quantum well (dot-dashed line) from Ref. 38 and for bulk GaN material (dot-dot-dashed line) from Ref. 39.

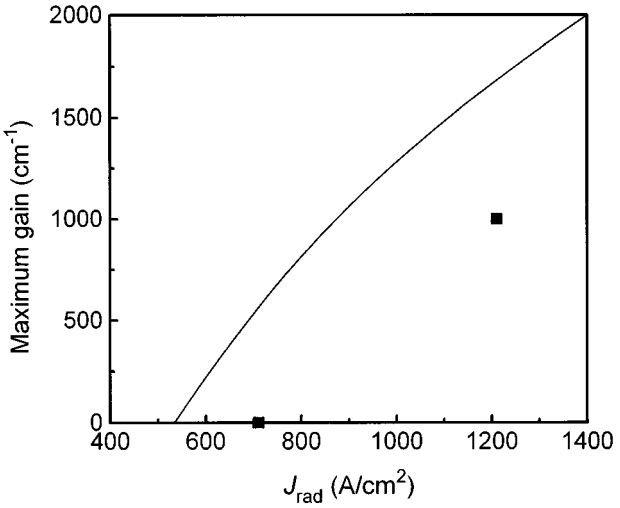

FIG. 12. Maximum optical gain of TE mode as a function of radiative current density for the GaN/$Ga_{0.85}Al_{0.15}N$ quantum well at $T=300$ K.

find that the compressive strain in the GaN well region strongly depresses the TM mode optical gain and enhances the TE mode optical gain. This can be understood as follows: comparing Fig. 1 with Fig. 4 shows that under compressive strain the energy separation between the **so1**+lh1 energy level and hh1 energy level increases. Therefore, the ratio of the number of **so1**+lh1 holes to the number of hh1 holes decreases. Consequently, the TM mode optical gain is depressed, because the TM mode optical gain is mainly contributed by the optical transitions between the **so1**+lh1 holes and the conduction subbands, as indicated in Fig. 6. Figure 9 shows that there is no positive TM optical mode gain even when the carrier density is as large as 10^{19} cm^{-3}. Consequently, the 100 Å well width GaN/$Ga_{0.85}Al_{0.15}N$ compressively strained quantum well laser diode is expected to only have a TE mode laser light output, if the injection carrier is not far beyond the above carrier density.

B. Maximum optical gain as a function of carrier density and J_{rad}

Figure 11 shows the maximum optical gain of TE mode as a function of carrier density for the GaN/$Ga_{0.85}Al_{0.15}N$ quantum well laser diode. Figure 12 shows the maximum optical gain of TE mode as a function of J_{rad} for the same laser diode. Meney *et al.* have also briefly reported in a letter[38] the optical gain calculation of 100 Å well width GaN quantum well with $Ga_{0.74}Al_{0.26}N$ barrier, using an 8×8 valence Hamiltonian and some assumed effective mass parameters. Their calculated maximum TE optical gain as a function of carrier density is also indicated in Fig. 11. The consistency between our work and Meney *et al.*'s work is reasonably good if we note that Meney *et al.* used a slightly different barrier material and they have not considered the strain effect in their curve. For comparison, we also show in Fig. 11 the maximum gain for a 100 Å GaAs/$Al_{0.4}Ga_{0.6}As$ quantum well.[38] As explained by Meney *et al.*, due to the larger effective mass of electron and hole in GaN, the transparency carrier density of GaN is larger than that of GaAs. In Fig. 12, two squares are also obtained from Meney *et al.*'s calculation for comparison. Fang *et al.* have calculated the optical gain of bulk GaN material.[39] Their calculation used simplified two-band model, neglecting the complication of the valence band structure and only heavy hole band is taken into account. Therefore, their result is qualitatively significant but quantitatively unreliable. In Fig. 11, Fang *et al.*'s result is also plotted for comparison.

The following points are noted in our work: (1) Owing to the lack of experimental data for GaN, we use the intraband relaxation time $\tau=0.1$ ps in Eq. (18), as usually utilized in GaAs materials.[28] However, due to the large structural defect density which may introduce a large number of scattering centers, the intraband relaxation time is expected to be reduced and this in turn reduces the quantum efficiency. (2) The large structural defect density also introduces a high density of deep trap levels in the energy gap. Many of these deep traps are nonradiative deep defects, which cause additional leakage current due to the nonradiative recombination between the electrons and holes. This has not been considered in our letter. (3) Chow *et al.* indicated that the excitonic effect due to the Coulomb interaction between electrons and holes contributes significantly to the magnitude of the optical gain.[40] We have not considered the excitonic effect in our calculation. However, their calculation is only for the bulk materials, and for simple parabolic heavy hole valence band. A more elaborate theoretical method which takes into consideration the coupling between heavy hole, light hole, and spin-orbit split-off hole in the quantum well, the strain effect and Coulomb interaction effect between the electrons and holes will be necessary to obtain more reliable quantitative results for the optical gain of an ideal GaN quantum well laser. On the other hand, improving growth techniques to reduce the defect density is essential for fabricating high quality GaN laser diodes.

VI. CONCLUSION

The valence hole subbands, TE and TM mode optical gains, transparency carrier density and radiative current density of the zinc-blende $GaN/Ga_{0.85}Al_{0.15}N$ strained quantum well (100 Å well width) have been investigated using a 6×6 Hamiltonian model including the heavy hole, light hole, and spin-orbit split-off bands. At the $k=0$ point, it is found that the light hole strongly couples with the spin-orbit split-off hole, resulting in the so+lh hybrid states. The heavy hole does not couple with the light hole and the spin-orbit split-off hole. The optical transitions between the valence subbands and the conduction subbands obey the $\Delta n=0$ selection rule. At the $k\neq0$ points, there are strong band mixing among the heavy hole, light hole, and spin-orbit split-off hole. The optical transitions do not obey the $\Delta n=0$ selection rule. The compressive strain in the GaN well region increases the energy separation between the so1+lh1 energy level and the hh1 energy level. Consequently, the compressive strain enhances the TE mode optical gain, and strongly depresses the TM mode optical gain. There is no positive TM mode optical gain even when the carrier density is as large as 10^{19} cm^{-3}. The TE mode optical gain spectrum has a peak at around 3.26 eV. The transparency carrier density is 6.5×10^{18} cm^{-3}, which is larger than that of GaAs quantum well. The compressive strain overall reduces the transparency carrier density. The J_{rad} is 0.53 kA/cm^2 for the zero optical gain. The results obtained in this work will be useful in designing quantum well GaN laser diodes and detectors.

ACKNOWLEDGMENTS

We would like to acknowledge the Computer Centre, National University of Singapore, and National Supercomputing Research Center, National University of Singapore for the use of supercomputers. This work was supported by National University of Singapore Research Grant No. RP 920621 and Singapore National Science and Technology Board RIC-University Research Project 681305.

[1] S. Nakamura, M. Senoh, S. Nagahma, N. Iwasa, T. Yamada, T. Matsushita, H. Kiyoku, and Y. Sugimoto, Jpn. J. Appl. Phys. **35**, 174 (1996).
[2] T. Lei, T. D. Moustakas, R. J. Graham, Y. He, and S. J. Berkowitz, J. Appl. Phys. **71**, 4933 (1992).
[3] S. J. Hwang, W. Shan, R. J. Hauenstein, and J. J. Song, Appl. Phys. Lett. **64**, 2928 (1994).
[4] A. Rubio, J. L. Corkill, M. L. Cohen, E. L. Shirley, and S. G. Louie, Phys. Rev. B **48**, 11810 (1993).
[5] E. A. Albanesi, W. R. L. Lambrecht, and B. Segall, Phys. Rev. B **48**, 17841 (1993).
[6] A. F. Wright and J. S. Nelson, Phys. Rev. B **50**, 2159 (1994).
[7] S. Strite and H. Morkoç, J. Vac. Sci. Technol. B **10**, 1237 (1992).
[8] K. Kim, W. R. L. Lambrecht, and B. Segall, Phys. Rev. B **50**, 1502 (1994).
[9] N. E. Christensen and I. Gorczyca, Phys. Rev. B **50**, 4397 (1994).
[10] *Proceedings of the 7th Trieste ICTP-IUAP Semiconductor Symposium*, edited by C. G. van de Walle [Physica B **185**, R9 (1993)].
[11] T. Lei, M. Fanciulli, R. J. Molnar, T. D. Moustakas, R. J. Graham, and J. Scanlon, Appl. Phys. Lett. **95**, 944 (1991).
[12] Z. Sitar, M. J. Paisley, J. Rnan, J. W. Choyke, and R. F. Davis, J. Mater. Sci. Lett. **11**, 261 (1992).
[13] P. E. Van Camp, V. E. Van Doren, and J. T. Deverse, Phys. Rev. B **44**, 9056 (1991).
[14] A. Munoz and K. Kunc, Phys. Rev. B **44**, 10372 (1991).
[15] M. A. Khan, R. A. Skogman, and J. M. Van Hove, Appl. Phys. Lett. **56**, 1257 (1990).
[16] S.-H. Ke, M.-C. Huang, and R.-Z. Wang, Solid State Commun. **89**, 105 (1994).
[17] S. Krishnankutty, R. M. Kolbas, M. A. Khan, J. N. Kuznia, J. M. Van Hove, and D. T. Olson, J. Electron. Mater. **21**, 437 (1992), *ibid.* **21**, 609 (1992).
[18] H. Grille and F. Bechstedt, Superlattices Microstruct. **16**, 29 (1994).
[19] G. Ramirez-Flores, H. Navarro-Contreras, A. Lastras-Martinez, R. C. Powell, and J. E. Greene, Phys. Rev. B **50**, 8433 (1994).
[20] D. A. Broido and L. J. Sham, Phys. Rev. B **31**, 883 (1995); *ibid.* **34**, 3917 (1986).
[21] R. People and S. K. Sputz, Phys. Rev. B **41**, 8431 (1990).
[22] A. T. Meney, B. Gonul, and E. P. O'Reilly, Phys. Rev. B **50**, 10893 (1994).
[23] J. M. Luttinger, Phys. Rev. **102**, 1030 (1956).
[24] W. J. Fan, M. F. Li, T. C. Chong, and J. B. Xia, J. Appl. Phys. **79**, 188 (1996).
[25] W. J. Fan, M. F. Li, T. C. Chong, and J. B. Xia, Solid State Commun. **97**, 381 (1996).
[26] E. A. Albanesi, W. R. L. Lambrecht, and B. Segall, J. Vac. Sci. Technol. B **12**, 2470 (1994).
[27] M. Fanciulli, T. Lei, and T. D. Moustakas, Phys. Rev. B **48**, 15144 (1993).
[28] M. Yamada and Y. Suematsu, J. Appl. Phys. **52**, 2653 (1981).
[29] W. J. Fan, M. F. Li, T. C. Chong, and J. B. Xia, Superlattices Microstruct. (to be published).
[30] J. N. Schulmann and Y. C. Chang, Phys. Rev. B **24**, 4445 (1981).
[31] J. B. Xia, Phys. Rev. B **38**, 8358 (1988).
[32] S. W. Corzine, R.-H. Yan, and L. A. Coldren, in *Quantum Well Lasers*, edited by P. S. Zory, Jr. (Academic, New York, 1993), p. 49.
[33] E. O. Kane, J. Phys. Chem. Solids **1**, 249 (1957).
[34] T. C. Chong and C. G. Fonstad, IEEE J. Quantum Electron. **25**, 171 (1989).
[35] F. Szmulowicz and G. J. Brown, Phys. Rev. B **51**, 13203 (1995).
[36] M. Asada and Y. Suematsu, IEEE J. Quantum Electron. **21**, 434 (1985).
[37] G. Lascher and F. Stern, Phys. Rev. **133**, A553 (1964).
[38] A. T. Meney and E. P. O'Reilly, Appl. Phys. Lett. **67**, 3013 (1995).
[39] W. Fang and S. L. Chuang, Appl. Phys. Lett. **67**, 751 (1995).
[40] W. W. Chow, A. Knorr, and S. W. Koch, Appl. Phys. Lett. **67**, 754 (1995).